A large disordered region confers a wide spanning volume to vertebrate Suppressor of Fused as shown in a trans-species solution study

Staëlle Makamte, Aurélien Thureau, Amira Jabrani, Annick Paquelin, Anne Plessis, Mathieu Sanial, Olga Rudenko, Francesco Oteri, Marc Baaden, Valérie Biou

Journal of Structural Biology 214 (2022) 107853

Contents lists available at ScienceDirect

Journal of Structural Biology

journal homepage: www.elsevier.com/locate/yjsbi

Research Article

A large disordered region confers a wide spanning volume to vertebrate Suppressor of Fused as shown in a *trans*-species solution study

Staëlle Makamte [a], Aurélien Thureau [b], Amira Jabrani [a], Annick Paquelin [a], Anne Plessis [c], Matthieu Sanial [c], Olga Rudenko [b], Francesco Oteri [d,1], Marc Baaden [d], Valérie Biou [a,*]

[a] Laboratoire de Biologie Physico-Chimique des Protéines Membranaires, Université de Paris, UMR 7099 CNRS, Institut de Biologie Physico-Chimique, 13 rue Pierre et Marie Curie, 75005 Paris, France
[b] Synchrotron SOLEIL, F-91192 Gif sur Yvette, France
[c] Université de Paris, CNRS, Institut Jacques Monod, F-75006 Paris, France
[d] Laboratoire de Biochimie Théorique, UPR 9080 CNRS, Institut de Biologie Physico-Chimique, 13 rue Pierre et Marie Curie, 75005 Paris, France

ARTICLE INFO

Keywords:
Hedgehog signal
Intrinsically disordered protein
Small-angle X-ray scattering

ABSTRACT

Hedgehog (Hh) pathway inhibition by the conserved protein Suppressor of Fused (SuFu) is crucial to vertebrate development. By constrast, SuFu loss-of-function mutant has little effect in drosophila.

Previous publications showed that the crystal structures of human and drosophila SuFu consist of two ordered domains that are capable of breathing motions upon ligand binding. However, the crystal structure of human SuFu does not give information about twenty N-terminal residues (IDR1) and an eighty-residue-long region predicted as disordered (IDR2) in the C-terminus, whose function is important for the pathway repression. These two intrinsically disordered regions (IDRs) are species-dependent.

To obtain information about the IDR regions, we studied full-length SuFu's structure in solution, both with circular dichroism and small angle X-ray scattering, comparing drosophila, zebrafish and human species, to better understand this considerable difference. Our studies show that, in spite of similar crystal structures restricted to ordered domains, drosophila and vertebrate SuFu have very different structures in solution. The IDR2 of vertebrates spans a large area, thus enabling it to reach for partners and be accessible for post-translational modifications. Furthermore, we show that the IDR2 region is highly conserved within phyla but varies in length and sequence, with insects having a shorter disordered region while that of vertebrates is broad and mobile. This major variation may explain the different phenotypes observed upon SuFu removal.

1. Introduction

The conserved Hedgehog (Hh) signalling pathway is essential to specify cell and tissue fate during embryogenesis and later to regulate stem cell homeostasis (Jiang and Hui, 2008). Discovered in drosophila, where it ensures proper polarisation of the larva segments (Nüsslein-Volhard and Wieschaus, 1980), the Hh pathway has since been identified in many animals where it controls multiple patterning events, and has rapidly emerged as a key player in oncogenesis by controlling tumour promotion or/and progression (Pak and Segal, 2016). In the absence of Hh signal the G-Protein Coupled Receptor-related Smoothened (Smo) activity is inhibited by the Hh receptor Patched (Ptc). Binding of Hh releases this negative effect, triggering the activation of Smo, probably by favouring its association with intramembrane cholesterol (for review see (Hu and Song, 2019)). Smo activation also involves its relocalisation from intracellular vesicles to the plasma membrane in drosophila, and its rapid translocation from the base to the tip of the primary cilium in mammals (Hooper and Scott, 1989; Ingham et al., 1991; Marigo et al., 1996; Zhang et al., 2018). Via its interactions with a cytoplasmic protein complex, Smo activates kinases that change the phosphorylation state of several proteins of this complex and remodel their interactions. As a result, the transcription factor(s) of the Ci/Gli family are activated and transported into the nucleus where they in turn activate the expression of specific target genes, thus changing the

* Corresponding author.
E-mail address: valerie.biou@ibpc.fr (V. Biou).
[1] Present address: Laboratoire de Biologie Computationnelle et Quantitative UMR7238 CNRS, Sorbonne Université, Institut de Biologie Paris-Seine, Bât. C, 4 place Jussieu, 75005 Paris, France.

https://doi.org/10.1016/j.jsb.2022.107853
Received 12 November 2021; Received in revised form 10 March 2022; Accepted 24 March 2022
Available online 29 March 2022

cell fate. The molecular backbone of the pathway is conserved but it becomes more complex from flies to mammals. For example in vertebrates, three transcription factors are involved: Gli 1, 2 and 3; their activation takes place at the primary cilium and depends on intraflagellar trafficking and results in their translocation into the nucleus (Huangfu et al., 2003).

The proper function of the Hh pathway at the right time and place is so crucial that several levels of negative regulation exist to prevent inappropriate Hh activation. This includes the products of two tumour suppressor genes: Ptc at the cell surface and Suppressor of Fused (SuFu) inside the cell. Removal of SuFu has very different consequences in drosophila and mammals. In drosophila, the phenotype of *sufu* removal is only visible in the context of the absence of *fused* kinase (Préat, 1992). Conversely, *SuFu* KO mice die in utero and exhibit heart, brain and CNS defects due to a Hh constitutional activation (Cooper et al., 2005; Svärd et al., 2006).

Discovered in drosophila (Préat, 1992), where it interacts with a microtubule-associated complex including kinase Fused (Monnier et al., 1998), SuFu is a 55 kDa protein that plays an inhibitory role via the sequestration of full-length Ci in the cytoplasm. In response to Hh, this negative effect of SuFu is suppressed by the kinase Fused. SuFu then accompanies Ci into the nucleus (Sisson et al., 2006). In zebrafish, SuFu regulates Gli transfer to the primary cilium (Maurya et al., 2013) and SuFu morpholino knock down affects eye, ear and muscle development, identifying SuFu as a medium-level inhibitor of the Hh pathway (Koudijs et al., 2005). In mammals, SuFu is essential for the proper differentiation of many cell types including neural cells (Yabut et al., 2015) and it plays a role in white/brown adipocyte determination and obesity (Pospisilik et al., 2010). Here also, SuFu acts upstream of the Gli transcription factors, controlling their fate. It was thus shown to sequester full-length Gli 1 and 2 transcription factors in the cytoplasm in the absence of Hh. Moreover, SuFu also plays nuclear roles with the repressor forms of Gli as it was shown to recruit the SAP18-mSin3 repressor complex to the Gli binding sites (Paces-Fessy et al., 2004). Hh binding to Ptc represses this negative effect, allowing the Gli proteins – accompanied by SuFu- to enter the nucleus. The present state of research describes SuFu as a hub, interacting with many partner proteins, and the interactions are remodelled when Hh is activated, mostly via post-transcriptional modifications, such as phosphorylation and ubiquitylation, of SuFu (Chen et al., 2011; Raducu et al., 2016; Wang et al., 2016).

Fig. 1 shows an amino acid sequence alignment of SuFu from three species belonging to different phyla: *Homo sapiens* (hSuFu), *Danio rerio* (zebrafish) (zSuFu) and *Drosophila melanogaster* (dSuFu). The crystal structures of hSuFu and dSuFu (Cherry et al., 2013; Zhang et al., 2013) harbour two ordered domains corresponding to the regions framed in blue and brown boxes in the Fig. 1; the N-terminal domain sequences have 41% identity, while the C-terminal domain has 24% identity between hSuFu, zSuFu and dSuFu. The N-terminal domain is also found in prokaryotic proteins, amongst which antitoxin systems, another process involving protein–protein interactions (Zhang et al., 2011), and the C-terminal domain is specific to SuFu proteins. In addition to those two domains known from the crystal structures, Fig. 1 shows that SuFu amino acid sequence contains two additional regions predicted to be intrinsically disordered by the PONDR server (https://www.pondr.com). We call the N-terminus disordered region IDR1 (in a dotted grey box) and the second region IDR2 (in a dotted black box) stemming from the C-terminal domains. These two regions harbour the most striking sequence differences between drosophila and vertebrates with 6% identical residues only.

The N-terminal domain has a 7-stranded twisted beta sheet followed by a 3-helix bundle, and spans residues 30–263 (as numbered in hSuFu). The C-terminal domain has two beta sheets with 6 and 4 strands respectively and two helices; it consists of residues 267–280 and 356–457. The structure of free hSuFu (pdb code 4KM9/4BL8) is extended and the two domains become close to each other when a peptide from Gli is bound to hSuFu (pdb code 4KMD/4BLB), showing a potential tendency of the two domains to move with respect to each other. The drosophila SuFu crystal structure pdb code 4KMA spans residues 13–259 for the N-terminal domain and 265–454 for the C-terminal domain. Both domains have very similar folds to the human protein, but their relative orientations are different. The IDR2 region, which is disordered in the human structure, has only twelve disordered amino acids in the drosophila crystal structure. The rest of the sequence corresponding to IDR2 is structured and caps the C-terminal domain, but it has no regular secondary structure. A solution small angle X-ray scattering (SAXS) study was performed on two fusion constructs

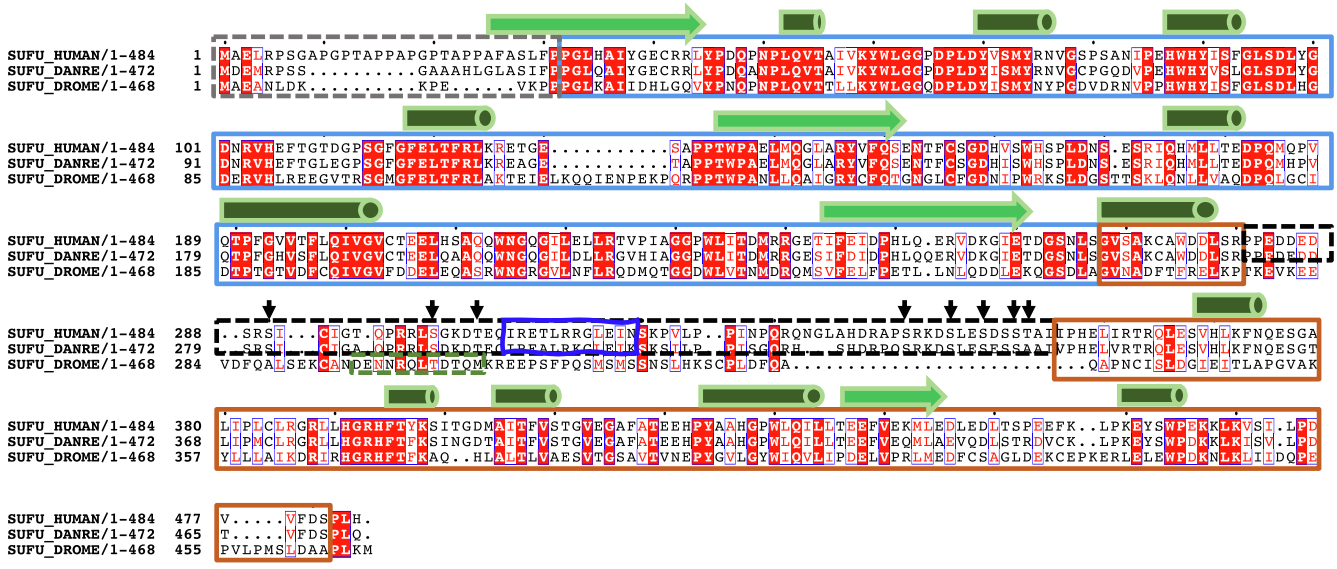

Fig. 1. Alignment of SuFu aminoacid sequences from *Homo sapiens* (human), *Danio rerio* (danre) and *Drosophila melanogaster* (drome), showing aminoacid numbering on the sides. Dotted grey box = IDR1; dotted black box = IDR2 for human and zebrafish; dotted green box = IDR2 for drosophila; N-terminal domain is in solid light-blue boxes and C-terminal domain is in solid brown boxes. The wavy blue box shows the nuclear export signal and arrows show phosphorylable serines in the vertebrate IDR2. Secondary structures observed in hSuFu crystal structure: Green cylinder = alpha helix; green arrow = beta strand. The alignment was done with T_coffee (Notredame et al., 2000) and enhanced with Espript (Gouet et al., 2003). IDR1 corresponds to residues 1–31, 1–20 and 1–15 for hSuFu, zSuFu and dSuFu, respectively, and IDR2 corresponds to residues 294–378, 272–356 and 384–394 for hSuFu, zSuFu and dSuFu, respectively.

consisting of maltose-binding protein (MBP) at the N-terminus of 32–483 hSuFu and of MBP-hSuFu deleted from residues 279–360 (corresponding to the IDR2). The derived *ab-initio* envelopes exhibit differences that can be assigned to the IDR2 (Cherry et al., 2013).

We sought structural information for full-length, biologically relevant, SuFu, using circular dichroism (CD) and SAXS to investigate the solution structures of SuFu proteins from *Drosophila melanogaster*, *Danio rerio* and *Homo sapiens*. We found that the solution structure of the drosophila protein is very similar to the crystal structure, and investigated its breathing movements by normal mode analysis. Human and zebrafish SuFu show similar dimensions and exhibit an N-terminal IDR1 region that seems to remain close to the N-terminal domain, while the IDR2 loop in the C-terminal domain spans a large volume and can thus fetch its partner protein a long way from its core. Our present studies show that, even though their crystal structures are quite similar, the solution structures of vertebrate and drosophila SuFu are rather different and we discuss the specificity of IDR2 in the context of SuFu interaction with partner proteins.

2. Experimental procedures

2.1. Protein expression and purification

dSuFu and hSuFu were cloned and expressed as previously described (Jabrani et al., 2017).

The cDNA encoding dSuFu was cloned in the pDEST17 (Invitrogen) expression vector according to standard Gateway™ protocols. The resulting plasmid encoded an N-terminal hexahistidine tag and a tobacco etch virus (TEV) protease cleavage site before the gene of interest. *E. coli* strain C41(DE3) (Miroux and Walker, 1996) were grown in 2YT medium at 37 °C until the optical density reached 0.6. Protein expression was induced with 0.2 mM isopropyl β-thiogalactoside overnight at 20 °C. Bacterial cells were recovered by centrifugation at 5000 g for 15 min and frozen at −80 °C. Similar procedures were used for the cDNAs encoding hSuFu and zSuFu respectively, which were cloned in a pACYDuet vector. Cells were lysed in 50 mM HEPES pH 7.5, 500 mM NaCl, 5 mM imidazole, 10% glycerol using a Constant Cell disruptor at 2.3 kbar, then centrifuged for 1 h at 9000g. The supernatant was loaded onto a Nickel affinity column (Roche), washed in the loading buffer and eluted in a buffer containing 200 mM imidazole. The eluate was collected and the buffer exchanged against 10 mM HEPES pH 7.5, 100 mM NaCl, 10 % glycerol, 2.5 mM $MgCl_2$ and 2 mM β-mercaptoethanol on a concentrator. Then the protein solution was incubated with Tobacco Etch Virus protease for 24 h at 10 °C to cleave the 6-Histidine tag and the associated linker. The cleavage mixture was then dialysed back into the lysis buffer and incubated with Nickel affinity gel (Roche) for one hour to separate the cleaved protein from the TEV protease and tag. The flow through was then concentrated and injected on a Superdex 200 10/300 gel filtration column equilibrated with HEPES 50 mM pH 7.5, NaCl 200 mM, glycerol 10%, Dithiothreitol 5 mM and loaded onto a HiTrapQ column, washed and eluted in a NaCl gradient. The fractions corresponding to pure SuFu protein were concentrated and used for future studies.

After TEV cleavage, the resulting aminoacid sequences used in this study correspond to the full-length aminoacid sequence with a Glycine at the N-terminus, resulting from TEV cleavage. The studied sequences are listed in Supplementary figure S1. They consist in 468 aminoacids for dSuFu, 484 for hSuFu and 472 for zSuFu with theoretical masses of 52.69, 53.9 and 52.71 kDa, respectively.

2.2. SRCD measurements

Synchrotron radiation circular dichroism (SRCD) was measured at the DISCO beamline (SOLEIL synchrotron, Gif sur Yvette, France). All sample concentrations were measured using the absorbance at 280 nm, after centrifugation and just prior to measurement, using a theoretical extinction coefficient of 59400 $M^{-1}.cm^{-1}$ for dSuFu, 67775 $M^{-1}.cm^{-1}$ for hSuFu and 66390 $M^{-1}.cm^{-1}$ for zSuFu. Concentrations were found to be between 4 and 10 mg/ml.

The beamline monochromator was calibrated using a camphorsulfonic acid solution prior to measurements. One microlitre of sample was deposited on one face of a calcium fluoride circular cuvette (Hellma), then the second face was carefully positioned and the cuvette closed by capillary force. Interferometry measurement showed the optical path to be 2.3 μm. The cuvette was placed in an airtight, metal sample holder that was positioned in the beamline Peltier temperature-controlled chamber, allowing for quick temperature changes with very little evaporation. Spectra were measured between 280 and 170 nm, each final spectrum being averaged from three repeated measurements. Thermal unfolding measurements were performed by averaging three spectra collected in steps of 5 °C between 10 and 90 °C. Buffer spectra were taken in the same conditions for subtraction from the protein spectra. Spectra were then processed for buffer subtraction and scaling using the CDTools program (Lees et al., 2004). The melting temperature was evaluated by fitting the curve displaying the CD at 208 nm with a sigmoidal function in Kaleidagraph (Synergy Software), as a function of temperature.

2.3. Size exclusion column coupled to multi-angle light scattering and refractometry (SEC-MALS) analysis

SEC-MALLS experiments for absolute mass determination of protein were carried out on a Shimadzu HPLC coupled to an Optilab® T-rEX™ refractometer and a miniDawn™ TREOS Multi Angle Laser Light Scattering (MALLS) detector (Wyatt Technology). The sample was injected in a Superdex 200 10/300 column for dSuFu and a Phenomenex 3000 HPLC column for hSuFu. The data were processed using the Astra software (Wyatt).

2.4. Small angle X-ray scattering measurements

The SAXS measurements were done at the SWING beamline (Thureau et al., 2021) at the SOLEIL synchrotron (Gif sur Yvette, France). The sample was injected at a flux of 0.3 ml/minute into an Agilent BioSEC-3–300 size exclusion column (dSuFu and zSuFu) or Waters BioResolve 2.5–200 (for hSuFu) pre-equilibrated in the indicated buffer and mounted on an HPLC system, prior to its analysis in the X-ray beam. The X-ray energy was 12 keV. For dSuFu, measurements were carried out with an Aviex charge coupled device detector, the system being programmed to measure 100 images of the buffer then 240 images of the protein, using a 1-second exposure time interspaced by 500 ms. For hSuFu and zSuFu measurements, an Eiger 4 M pixel detector was used. 600 images were measured with 990 ms exposure and 10 ms dead time each. The sample to detector distance is listed in Table 2.

The images were processed using the FOXTROT software (https://www.synchrotron-soleil.fr/en/beamlines/swing) developed at the SOLEIL synchrotron. The curves derived from buffer measurement were averaged and subtracted from the sample curves. Then the Guinier q-range was estimated on the most intense curve and a radius of gyration (Rg) was calculated using a Guinier plot for all subtracted scattering curves, thus producing a plot of Rg and scattered intensity, I_0, for all frames. Curves from hSuFu and zSuFu were processed with US-SOMO (Brookes et al., 2016) to deconvolute the contribution from oligomers. The curves obtained from dSuFu did not indicate higher order species and consequently did not need deconvolution. The subtracted frames, corresponding to the deconvoluted peak with a stable Rg, were selected to produce the protein scattering curve of scattered intensity as a function of the momentum transfer $q = 4\pi\sin(\theta)/\lambda$, where 2θ is the diffusion angle and λ is the wavelength. Further analysis (Guinier and Kratky plots, Radius of gyration Rg and intensity at origin I_0 calculation) was performed with the ATSAS program suite (Franke et al., 2017).

2.5. Molecular modelling of dSuFu

The dSuFu crystal structure 4KMA was modified into an open conformation using Rosetta, (Kaufmann et al., 2010) based on the hSuFu structure (pdb ID 4KM9), as a template for relative domain orientation. This model structure, and the crystal structure 4KMA for dSuFu, were used as the initial and final frame, respectively, to guide a linear morphing obtained through the program Chimera (Pettersen et al., 2004). Each of the 20 morphing frames has been minimised without any constraint using the AMBER force field as implemented in Chimera (Pettersen et al., 2004). The 20 frames have then been analysed through the program Foxs (Schneidman-Duhovny et al., 2013) in order to calculate the corresponding scattering curve and its agreement with experimental data. The frame with the curve having the lowest chi^2 value with respect to the experimental data was retained as the experimental model.

2.6. Molecular modelling of hSuFu missing regions

hSuFu residue numbering is according to Uniprot entry Q9VG38. Our SAXS data was measured on full-length hSuFu. The crystal structure of hSuFu PDB code 4KM9 was used as a starting point. It shows two ordered domains, but the first 20 aminoacids (IDR1) and 76 residues (IDR2) in the C-terminal domain are disordered. Modeller (Fiser et al., 2000; Šali and Blundell, 1993) was used to generate 20 models with missing residues, amongst which five were chosen to have IDR2 structures with different shapes. The chi^2 of the calculated scattering curve with respect to the experimental curve ranged between 1.58 and 6.32 with an average of 3.8. The five models were then submitted to Dadimodo server https://dadimodo.synchrotron-soleil.fr (Rudenko et al., 2019) for a refinement against the SAXS data by introducing flexibility in the IDR1 and the IDR2 and in the linker between the domains. The two ordered domains: residues 30–255 for the N-terminal domain and residues 259–268 and 356–472 for the C-terminal domain were kept rigid while residues 1–29, 256–258 and 269–355 were left flexible. Five models were generated for each starting model and ranked according to the chi^2 value. Another test was performed with a closed model starting from structure 4KMD on which the HDR1 and HDR2 regions obtained from the refined hSuFu structure were grafted. A third calculation used AlphaFold2 model Q9UMX1 of hSuFu as a starting point for Dadimodo.

2.7. Molecular modelling of zSuFu

zSuFu was modelled by homology using the Phyre2 server (Kelley et al., 2015). The best-ranked model was based on hSuFu structure PDB code 4KMH. Then missing residues in the IDR2 loop (73 residues) were added with Modeller, generating twenty models, amongst which five were chosen to have loops structures with different shapes. The chi^2 of the calculated scattering curve with respect to the experimental curve ranged between 1.91 and 40 with an average of 12.6 and a median of 5.4. The five models were processed with Dadimodo, with residues 18 – 255 for the N-terminal and residues 259 – 268 and 356 – 472 for the C-terminal domain being kept rigid while residues 1–19, 256–258 and 279–355 were left flexible. Five models were generated for each starting model and ranked according to the chi^2 value.

3. Results

3.1. Synchrotron radiation circular dichroism (SRCD) shows that human SuFu is more stable than zebrafish and drosophila SuFu

We measured SRCD spectra between 10 and 90 °C for dSuFu, hSuFu and zSuFu in buffer HEPES HCl 50 mM pH 7.5, NaCl 200 mM, glycerol 10%, Dithiothreitol 2 mM. All proteins showed spectra typical of structured proteins at low temperature, and the spectra became shallower when the temperature was increased, (Fig. 2 A-C). The spectra cross at an isobestic point characteristic of a two-state transition.

Plotting the minimum CD value at 208 nm as a function of temperature results in sigmoid-like curves (Supplementary Figure S2). The transition temperatures were calculated using a sigmoidal fit in Kaleidagraph software with the following equation:

$$CD208(T) = CDmin + (CDmax - CDmin) \Big/ \left(1 + (T/Tm)^k\right)$$

where CDmin and CDmax are the minimum and maximum values of CD208; T is the temperature; Tm is the transition temperature (corresponding to the inflexion point of the curve); k is the slope variable. The obtained values of Tm are 40.7 °C for dSuFu, 56.5 °C for hSuFu and 47.8 °C for zSuFu. We do not have an explanation for the difference in Tm, but we observe that drosophila and zebrafish are organisms with lower body temperature regulation than human, and their Tm are lower than those of hSuFu.

Table 1 shows the evaluation of secondary structure content using the BestSel program (Micsonai et al., 2015) at 10 and 60 °C. At low temperature, our SuFu constructs contain between 40 and 50% of regular secondary structure and the other residues are in random coil. All studied SuFu constructs become richer in beta strand and lose helical structure when the temperature is raised from 10 to 60 °C. This trend is observed in other helix-containing proteins such as myoglobin (Fändrich et al., 2003).

3.2. Sec-SAXS and molecular modelling show that dSuFu is an elongated monomer in solution with a closed conformation

SEC-MALS measurements showed that dSuFu has a mass of 55 kDa, consistent with a monomer in solution (Supplementary Figure S3A). The SAXS measurements were conducted at the SWING beamline at the SOLEIL synchrotron, using a High Pressure Liquid Chromatography injection system (Thureau et al., 2021).The sample migrated on the size exclusion column, and produced a peak with a homogeneous radius of

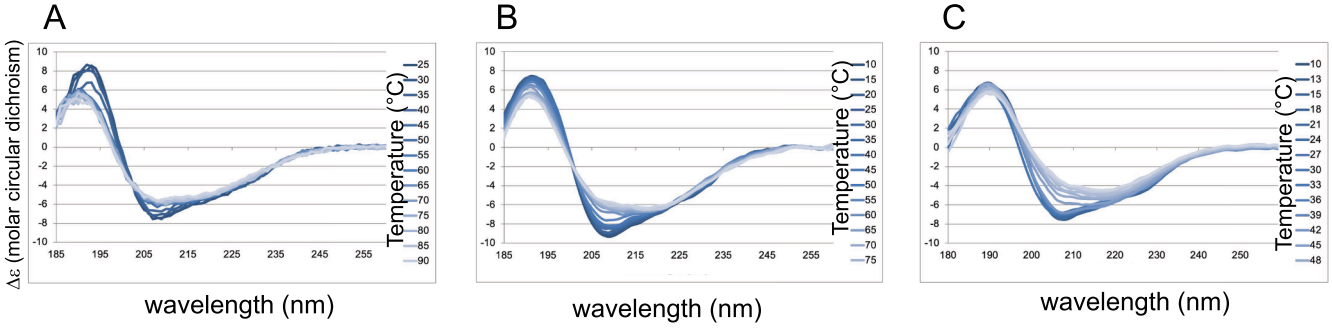

Fig. 2. SRCD measurements of SuFu from different species showing thermal unfolding. Spectra are colored with blue shades according to the temperature. A, dSuFu; B, hSuFu; C, zSuFu.

Table 1
Secondary structure variation upon thermal denaturation. The percentage of secondary structure evaluated by BestSel at 10 °C and 60 °C is indicated for alpha helix, beta strand and other secondary structures; the last three columns display the differences between 60 and 10 °C.

	Helix 10°	Helix 60°	Beta 10°	Beta 60°	Others 10°	Others 60°	Helix (60-10°)	Beta (60-10°)	Others (60-10°)
dSuFu	15.0	4.9	26.3	30.0	57.4	61.3	−10.1	3.7	3.9
hSuFu	31.2	16.9	6.9	17.8	61.9	65.3	−14.4	11.0	3.4
zSuFu	24.2	7.9	21.3	38.1	54.5	54.0	−16.2	16.7	−0.5

Table 2
SAXS data for dSuFu, hSuFu, and zSuFu. Rg = radius of gyration; Dmax = maximum interatomic distance; qRg_{max} = abscises of the maximum value for the normalised Kratky plot shown in Fig. 3B.

Sample	dSuFu	hSuFu	zSuFu
Data collection parameters			
Beamline	Swing beamline, SOLEIL synchrotron (France)		
Energy (keV)	12.0	12.0	12.0
Sample-detector distance (mm)	1804	2000	2000
q-range (Å-1)	0.008–0.5	0.008–0.5	0.008–0.5
Exposure time	1 s	990 ms	990 ms
Detector	Aviex charge coupled device	Eiger 4 M	
Software			
Primary data reduction	Foxtrot		
Data processing	US-SOMO		
Ab initio analysis	GNOM V5.0		
Computation of model intensities	Pepsi-SAXS		
Model building	4KMA + Modeller	4KM9 + Modeller	Phyre + Modeller
Model refinement	Dadimodo	Dadimodo	Dadimodo
Structural parameters			
Number of aminoacids	468	484	472
Theoretical mass (kDa)	52.69	53.9	52.71
Rg frm Guinier (Å)	27.2	36.0	33.7
I0 (cm^{-1})	0.017	0.03	0.05
qRgmax	1.27	1.2	1.2
Dmax from P(r) (Å)	90	150	150
Rg from P(r) (Å)	27.3	38.1	36.1
I0 from P(r) (cm^{-1})	0.017	0.03	0.05
Chi^2 Gnom	2.0	1.56	1.68
Dmax/Rg	3.3	4.2	4.4
qRgmax (Kratky)	1.6	2.0	2.1
qopt ($Å^{-1}$) (Shannon)	0.61	0.52	0.49

gyration (Rg) (Supplementary Figure S4A) which allows us to say that the resulting SAXS curve of dSuFu (Fig. 3A, brown curve) corresponds to a monodisperse solution of particles. The estimation of the Rg using the Guinier approximation indicates an absence of aggregates and gives an Rg value of 27.2 Å. The Shannon sampling formalism indicates that the data is accurate at least up to a scattering vector of 0.4 $Å^{-1}$. Table 2 gives a list of all measured values. The dimensionless Kratky plot (Fig. 3B, brown curve) has a bell shape and does not rise at high angles, which denotes that dSuFu has a mostly compact structure with very little disorder. The distance distribution function, P(r), calculated using an indirect Fourier transform, yielded a well-behaved curve with a maximum particle dimension, D_{max}, of 90 Å and a maximum of the curve at r = 35 Å (Fig. 3C, brown curve). The calculated mass of 51 kDa, obtained with Primus and Vc calculation (Rambo and Tainer, 2013), and the Rg values of 27.2 Å and 27.3 Å calculated from the Guinier and P(r) functions, respectively confirm that the particle is a monomer and is monodisperse in solution.

The average envelope resulting from *ab initio* calculations encloses most of the crystal structure of dSuFu 4KMA with the exception of the 274–282 loop, which is mobile in the crystal structure, as shown by the thinner radius of the ribbon representation corresponding to a higher B-factor (Fig. 4A). This figure highlights the IDR2 region that lines the C-terminal domain (residues 308–340 on the bottom left of the figure). It is ordered but it has no regular secondary structure.

The scattering curve calculated from the 4KMA crystal structure (Zhang et al., 2013) fits rather well with the SAXS spectrum, however the chi^2 value is 53.3 and there is some disagreement between 0.15 and 0.25 $Å^{-1}$ q value (Fig. 4B, blue experimental curve, compare with 4KMA green curve). We performed a modelling study in order to better characterise possible movements in dSuFu and find a model that fits the SAXS data better. The following two-step procedure was applied. First, we analysed the possible deformations in the SuFu structures. Wide rearrangements likely accounting for a conformational change in the dSuFu crystal structure have been inferred through hinge detection and

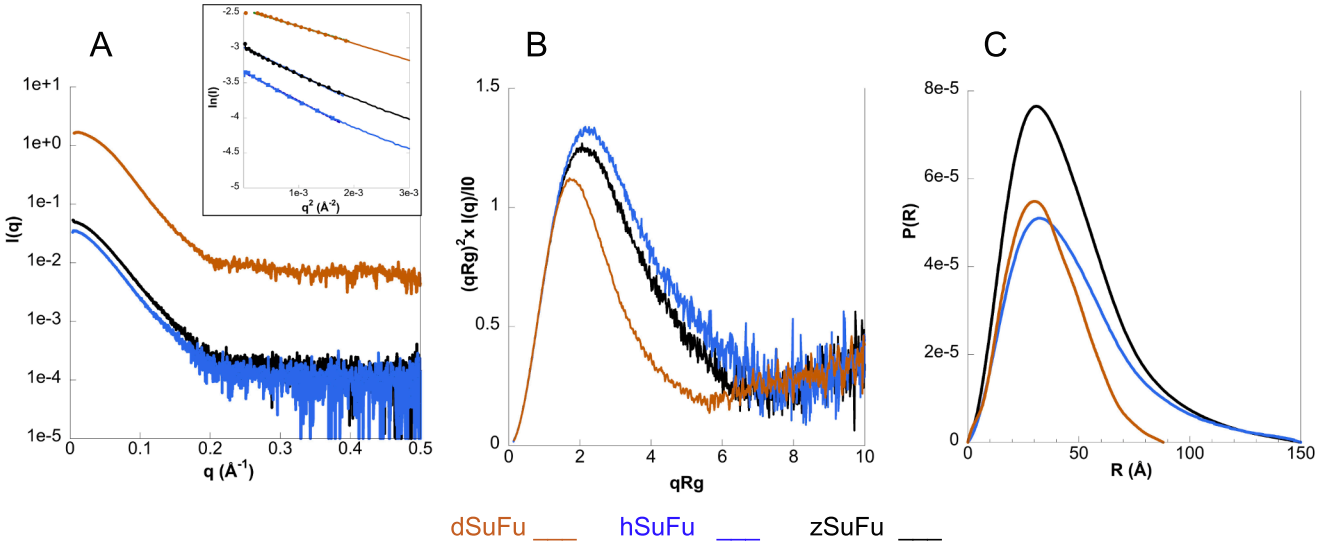

Fig. 3. SAXS studies of dSuFu (brown), hSuFu (blue), and zSuFu (black). A, SAXS scattering curves. The insert shows the Guinier regions; B, dimensionless Kratky plots; C, pair distance distribution P(R).

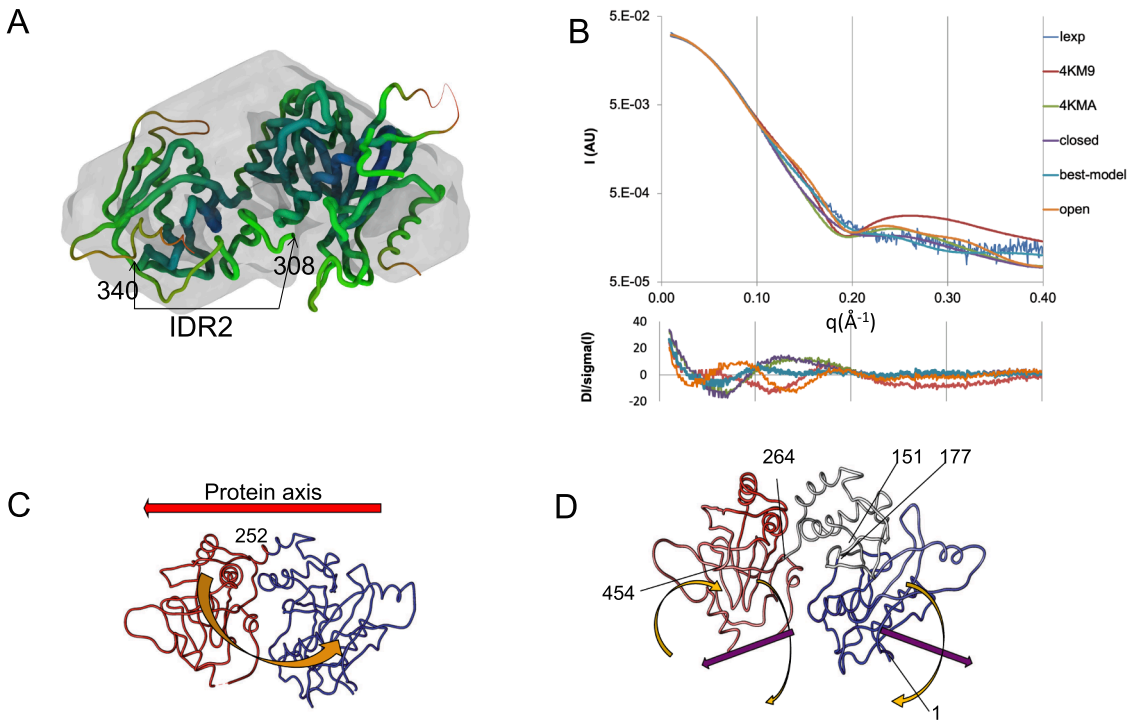

Fig. 4. SAXS structure of drosophila SuFu. A, superposition of the crystal structure 4KMA and the envelope calculated by GASBOR and DAMAVER suite. The structure is displayed using a worm-like representation with a radius inversely proportional to the B-factor in the PDB file. B, scattering curves superposed using Pepsisaxs (top) and their differences (bottom). The experimental curve is in light blue, the PDB models 4KM9 (hSuFu) in red, 4KMA (dSuFu) in mustard green, the three models used in the normal mode simulation: closed in green, open in orange and best model in purple. C, D, the two slowest modes of movement calculated by Hingeprot. The colours distinguish the domains moving relative to each other and the arrows show the direction of movements.

compared with hSuFu crystal structures. For each structure, the Hingeprot program (Emekli et al., 2008) shows the two slowest modes of movement. For the 4KMA crystal structure, the slowest mode describes the bending of the two domains around residues Q252-D253 (Fig. 4C). The second mode is described by three rigid blocks, namely N-terminal (M1 to C151 and Q177 to C194), central (Y152 to A176, and Q195 to A263) and C-terminal (G264 to E454), coloured in blue, white and red, respectively, in Fig. 4D. The N- and C-terminal domains also describe a bending motion, but here the domains do not pivot on the same hinge because of the rigidity of the central block (see magenta arrows in Fig. 4D). Additionally, a wide fluctuation is observed in the loop A105-P128.

In the next step, we sampled the movements of the two domains along the direction of the bending mode in order to check if a better agreement with our SAXS results can be obtained by modelling an intermediate on this bending pathway. Two extreme open and closed conformations were generated for dSuFu, using the open (4KM9) and closed (4KMD) conformations of hSuFu as templates. The conformational change from one state to the other was modelled using linear morphing, and twenty additional intermediate conformations were generated, each of which was regularized through energy minimization, (see materials and methods section). The SAXS profiles were then simulated for each of these energy-minimised conformations and compared to the experimental profile. Chi^2 values calculated up to a q value of 0.4 Å^{-1} are as follows: open model, 25.0; closed model, 59.3; 4KM9, 42.2; 4KMA, 53.3; best model, 14.1. The intermediate model whose scattering curve was closest to the SAXS data was selected as the best solution (Fig. 4B purple curve). This best model and the 4KMA structure of dSuFu have an RMSD of 0.7 Å for all backbone atoms. The differences mostly concern the C-terminal domain whose RMSD, with respect to the crystallized counterpart, is 0.9 Å versus 0.4 Å for the N-terminal domain. Although the secondary structure is globally conserved between the proposed solution model and the crystal structure, the residues ranging from A294 to D332 in the latter are more closely packed in the domain core. The higher flexibility of these residues, containing the unresolved loop D296 – K308, accounts for a widening of the cleft between the two domains as shown by the minimum distance between the two domains (5 Å between G133-Q302 C-alpha of 4KMA structure versus 11 Å of the equivalent G147-R309 in the model). Finally, we used Dadimodo server to refine models for dSuFu starting from our best model and defined a flexible linker between the two domains consisting of residues 256–265, leaving the C-terminal domain free to move with respect to the N-terminal domain. The five resulting structures are highly similar to each other and have an average chi^2 of 1.81 ± 0.04 (Fig. 5 A-B and Table 3).

In summary, SAXS measurements show that the solution structure of dSuFu is slightly more open than the 4KMA dSuFu crystal structure, but is nevertheless different from the free human protein 4KM9. In addition, hinge detection shows that the clamp mode likely characterises dSuFu motion. Finally, the region corresponding to IDR2 caps the C-terminal domain and is not disordered in the drosophila protein.

3.3. *Sec-SAXS shows that the IDR2 disordered region spans a large volume for hSuFu and zSuFu*

We chose to compare proteins from vertebrates that are far from each other in evolution: zebra fish and human. hSuFu shows 36% identity with dSuFu and 81% identity with zSuFu, while zSuFu has 35% identity with dSuFu (Fig. 1). As for dSuFu, we measured SEC-MALS on purified hSuFu and SEC-SAXS data on purified hSuFu and zSuFu. A reducing agent was necessary to remove a dimer-like species at pH7.5, coherent with the neutral pKa of cysteine protonation. We suspect that, above this pKa, a disulphide bridge is formed involving Cysteine 292 located in the IDR2 (data not shown).

The mass derived from SEC-MALS measurements of hSuFu (supplementary figure S3B) is of the order of 55 kDa, consistent with a

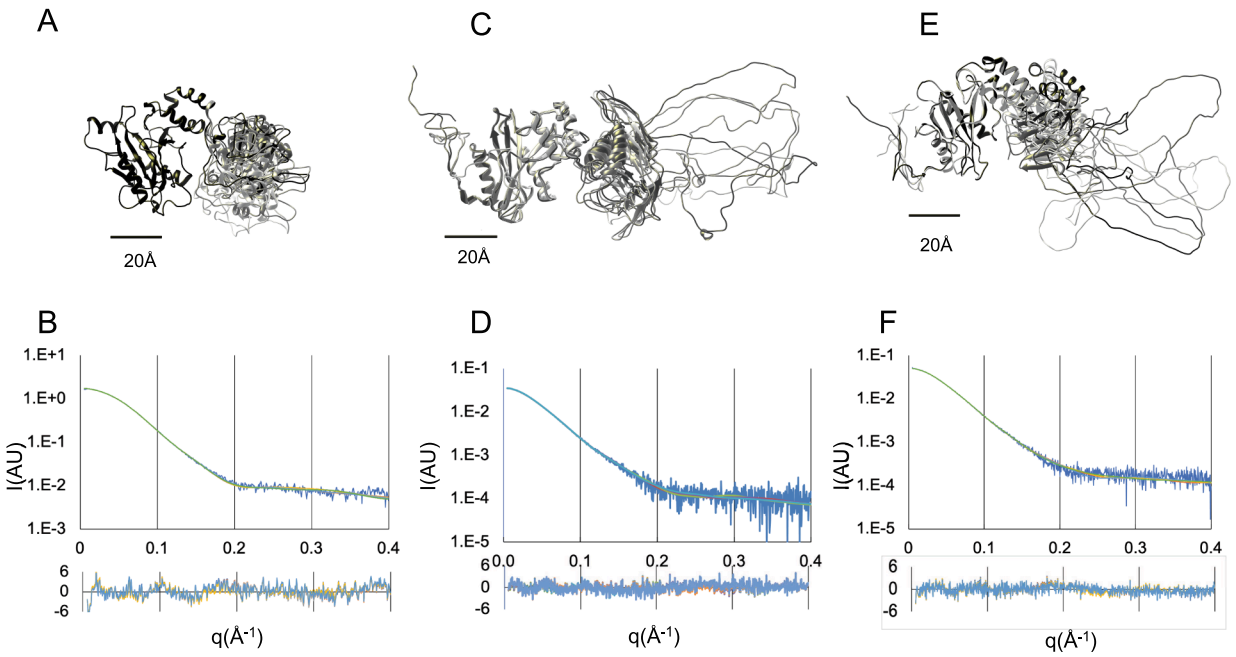

Fig. 5. Modelling of SuFu using Dadimodo and SAXS scattering curves. dSuFu (A-B) hSuFu (C-D), zSuFu (E-F) from SAXS data. A, C, E: Five best models from Dadimodo; B, D, F: fitting of experimental and model scattering curves (upper plots). The bottom plots correspond to the residual: ΔI/sigma(I).

Table 3
Atomistic modelling of structures from SAXS data: Pepsi-SAXS (Grudinin et al., 2017) comparison between experimental curve and that calculated from the Dadimodo output (5 best structures).

sample	dSuFu	hSuFu	zSuFu
q range ($Å^{-1}$)	0.008–0.4	0.008–0.4	0.008–0.4
Chi^2	1.80 ± 0.04	1.27 ± 0.08	1.18 ± 0.06
Hydration shell contrast Dro (e- $Å^3$)	0.03	0.03	0.03
Ra Å	1.617	1.615	1.615

monomeric state of this protein whose theoretical mass is 52.7 kDa.

The SEC-SAXS measurements were performed similarly to that described for dSuFu. The sample migrated on the size exclusion column, and appeared as a peak with a slight shoulder, and after a deconvolution using US-SOMO, produced a homogeneous radius of gyration (Rg) across the peak (Supplementary Figures S4 B and C), which allows us to say that the resulting SAXS curves of hSuFu and zSuFu (Fig. 3A, blue and black curves) correspond to a monodisperse particle. The Shannon sampling formalism shows that all curves can be used at least up to 0.4 $Å^{-1}$ (Shannon and Weaver, 1949). The Guinier region of the scattering curves are shown as inserts on Fig. 3A and the radii of gyration (Rg) values are listed in Table 2. The Rg of hSuFu is 36 Å, much larger than that of dSuFu (27.2 Å) for monomeric proteins of similar molecular weights.

The dimensionless Kratky curve of dSuFu has a maximum at x (qRg) equal to 1.73 and y equal to 1.1, corresponding to a globular protein, while the maximal x values of hSuFu and zSuFu are above 2.1 for a y equal to 1.25 and 1.30 respectively (Fig. 3B). In agreement with their higher Rg, this shift indicates that hSufu and zSufu conformations in solution are more elongated than the dSuFu conformation.

The P(R) curves have Dmax values of 90 Å for dSuFu while those of hSuFu and zSuFu are 150 Å (Fig. 3C), confirming that hSuFu (blue curve) and zSuFu (black curve) span a much larger volume than dSuFu (brown curve). Indeed, while all proteins have comparable molecular weights, the radius of gyration is 25% higher in hSuFu and zSuFu than for dSuFu. This is in agreement with the presence of the disordered IDR2 in zebrafish and human, which is ordered and folded over the domains in drosophila.

We went on to generate molecular models of SuFu whose calculated scattering curves fit the experimental curve well. We used the Dadimodo software (Rudenko et al., 2019) to find models that fit the experimental curve better. For hSuFu, we ran Dadimodo from three sets of starting models. A) As explained in the Methods section, we started from the free hSuFu crystal structure (pdb id 4KM9 (Zhang et al., 2013)) and built the missing regions using Modeller. We thus generated twenty structures, amongst which we chose five with the most different loops as starting points for Dadimodo. Fig. 5C shows the superposition of the five best output models. The fit between the model and the experimental scattering curves is very good with an average chi^2 value for the Dadimodo output models is 1.27 ± 0.08 (Table 3 and Fig. 5D). The N-terminal and C-terminal domains are in open conformation with respect to each other and the IDR1 residues seem to have a rather compact structure. This is different from the IDR2 loops that protrude a long way (up to 65 Å) into the solvent, conferring a very elongated structure to hSuFu. B) We also used the Alphafold2 (Tunyasuvunakool et al., 2021) model of hSuFu (id Q9UMX1) as a starting structure for Dadimodo. This model is very similar to free hSuFu crystal structures 4KM9 and 4BL8, i.e., the two domains are in open conformation with respect to each other. The chi^2 of the original model with respect to our SAXS curve was 6.02, and Dadimodo models brought it to an average chi^2 of 5.2. Supplementary Figure S5 shows a superposition between Q9UMX1 and our best hSuFu model, using the C-terminal domain as a reference. Alphafold2 added ordered secondary structures to the IDR2 (colored yellow): a fourth beta strand added to the second sheet of the C-terminal domain and an alpha helix between the two domains. This makes the IDR2 much more compact, while the IDR1 is more extended than in our models. This conformation, although it looks realistic, does not fit our solution SAXS curve well, in particular its Rg is 30.6 Å, significantly lower than our experimental Rg of 36 Å. C) In addition, we generated a starting model with closed domains similar to those of dSuFu whose domains are more closed with respect to each other even in the absence of the Gli peptide ligand. We thus generated a closed starting model using the Gli peptide-bound conformation of hSuFu (pdb id 4KMD) on which the missing regions were attached similarly to the extended model. We ran Dadimodo starting from this closed model. The resulting models have an average chi^2 of 2.80 ± 0.3. Their fit is significantly less good than those of the elongated models, showing that this set of conformations is less

probable in solution. However, we cannot exclude that the protein spends part of its time in this closed conformation.

In summary, hSuFu has a very elongated conformation in solution, compatible with an open conformation of the two ordered domains and an extended IDR2.

Finally, we studied zSuFu, the ortholog from another vertebrate species in order to compare it with hSuFu. The SAXS data for zSuFu confirm that the solution structure of zSuFu is very similar to that of human SuFu, both in terms of Rg and Dmax (Table 2) and significantly different from those of dSuFu. In order to obtain an atomic model of zSuFu, we produced a homology model using Phyre server based on pdb id 4KMH. We produced twenty models by adding the missing residues corresponding to IDR1 and IDR2 using Modeller and selected the five most different ones as starting points for Dadimodo. The five Dadimodo refined models have extended IDR2 loops similarly to hSuFu models (Fig. 5E) and have low chi^2 values of 1.18 ± 0.06 (Fig. 5F and Table 3). Thus, our SAXS data show that zSuFu has a solution structure similar to those of hSuFu.

In summary, our SAXS measurements provide structural data that the crystal structures do not supply. They show that drosophila SuFu has a very different shape in solution than vertebrate SuFu. This difference is mainly due to the presence of an extended IDR2 similar in both human and zebrafish species.

3.4. Aminoacid composition in the IDR2 is different from that of the overall sequence

The IDR2 loop thus contributes strongly to the large values of Rg and D_{max} of those proteins, and we investigated its amino acid composition in order to predict how the IDR2 of other species might behave. The IDR2 is 76 and 73 residue-long in human and zebrafish, respectively.

In the sequences aligned in Fig. 1, the IDR2 starts with an aromatic residue W/F (W275 in human) belonging to the first strand of the first ß-sheet of the C-terminal domain. This aromatic establishes contacts that stabilise the interaction with conserved hydrophobic residues in the second ß-sheet. The last residues in the IDR2 are the first ones of this ß-sheet and they ensure the stabilisation of the loop ends. The amino acid composition of SuFu sequences as displayed in Table 4 shows that the IDR2, as compared to the overall sequence, is richer in acidic residues and, to a lesser extent, in basic and polar residues, and poorer in hydrophobic residues, as could be expected from the nature of IDRs.

Table 4
Amino acid composition of the three SuFu sequences displayed in Fig. 1. The percentages are calculated using the Protparam server (https://web.expasy.org). The first column corresponds to all amino acids of the sequences; the second column corresponds to the IDR2 aminoacids as shown in the dotted black box on Fig. 1. The third column is the difference between the IDR2 and the overall composition.

aminoacid	% overall	% IDR2	%IDR2-%overall
A	5.38	5.12	−0.26
C	1.61	2.33	0.72
D	6.50	8.84	2.34
E	7.62	9.30	1.69
F	3.84	1.40	−2.45
G	7.55	3.26	−4.29
H	3.14	1.86	−1.28
I	4.82	6.51	1.69
K	3.91	6.05	2.13
L	10.76	7.44	−3.32
M	2.10	1.40	−0.70
N	3.00	3.72	0.72
P	8.04	8.37	0.34
Q	5.17	6.51	1.34
R	5.31	8.84	3.53
S	6.92	13.95	7.04
T	5.24	3.72	−1.52
V	5.10	1.40	−3.71
W	1.82	0.00	−1.82
Y	2.17	0.00	−2.17

4. Discussion and conclusion

Our solution investigation disclosed differences between drosophila and vertebrate SuFu that could not be anticipated from their respective crystal structures. Our SAXS results show that the closed conformation of dSuFu is not due to crystal packing effects but is intrinsic to dSuFu. Our modelling results indicate that this may be due to different hierarchy in the hinge motions, leading to a different equilibrium position. In addition, the sequence corresponding to the Intrinsically Disordered Region IDR2 is mostly ordered in drosophila, thus stabilising the two domains in this closed conformation. This poses the question of how dSuFu opens to bind its partner transcription factor Ci.

The hSuFu protein has an elongated monomeric structure and based on the crystal structures (Cherry et al., 2013; Zhang et al., 2013), our SAXS data allowed us to build models for the missing residues at the N-terminus and in the C-terminal domain. Those models suggest that the IDR2 forms an elongated loop that protrudes up to 65 Å into the solvent. This is comforted by the study of zSuFu, which is 81% identical in amino acid sequence to hSuFu and whose SAXS-derived size and shape are very similar to that of hSuFu.

Cherry and colleagues compared the SAXS profiles of hSuFu coupled to the maltose binding protein in presence and absence of the IDR2 region. They observed an increase in the Rg and Dmax values and modeled the IDR2 in a protrusion of the *ab initio* envelope as a disordered loop similar to our models. In addition, they performed hydrogen/deuterium exchange studies of two constructs: in the presence and in the absence of the IDR2 region (Cherry et al., 2013). They find some increase in the protection of the C-terminal domain, suggesting that the IDR2 can fold back onto the main body of hSuFu. The Alpha Fold2 model of hSuFu is compatible with this interaction. Our models with extended loops fit our SAXS data much better than the Alpha Fold2 model; however, it is possible that the IDR2 undergoes transient interactions with the main body that can be further stabilized by partner proteins.

The elongation of the IDR2 loop in vertebrates might be associated with an increased complexity in the Hh pathway from flies to vertebrates. This is exemplified by the transcription factor Ci that is unique in drosophila, while three Gli proteins are simultaneously present in mammals: Gli1, Gli2 and Gli3 (Ruppert et al., 1988), allowing fine-tuning of the gene expression pattern via other partner proteins.

The function of the IDR2 region is not well known. However, Cherry et al. have studied the effect of its removal on the Hedgehog pathway activation. They used a luciferase reporter in HEK cells and found that the IDR2 is dispensable for Gli binding and Hh pathway repression. An IDR2-truncated form and a chimeric human hSuFu harboring drosophila IDR2 were able to repress the Hh pathway, but failed to reactivate it when Smo agonist SAG was added (Cherry et al., 2013). This confirms that the IDR2 of vertebrate SuFu has a role in the regulation of the Hh pathway, likely linked to post-translation modifications and nuclear trafficking. The “Phosphosite” data base (Hornbeck et al., 2004) indicates that ten out of sixteen post-transcriptional modifications of hSuFu occur in the 80 aminoacids of the IDR2. Six serine and threonine residues are predicted to be phosphorylated and three lysines are predicted to be ubiquitylated or acetylated (Akimov et al., 2018).

Moreover, Zhang et al. showed that the mammalian SuFu harbors a nuclear export signal spanning residues 308–318 and two phosphorylatable serines 342 and 346 (Zhang et al., 2017). As shown on Fig. 6, those residues are located in the IRD2 making them very accessible to interact with kinases, ubiquitine ligases and the nuclear pore complex. This property makes the IRD2 a very good candidate to interact with exportins similarly to the complex between exportin CRM1, Ran-GTP and import adapter snurportin1 (SPN1), that involves disordered regions of SPN1 in contact with CRM1 (Monecke et al., 2009). Alternatively, the IDR2 could gain in secondary structure as hinted by the

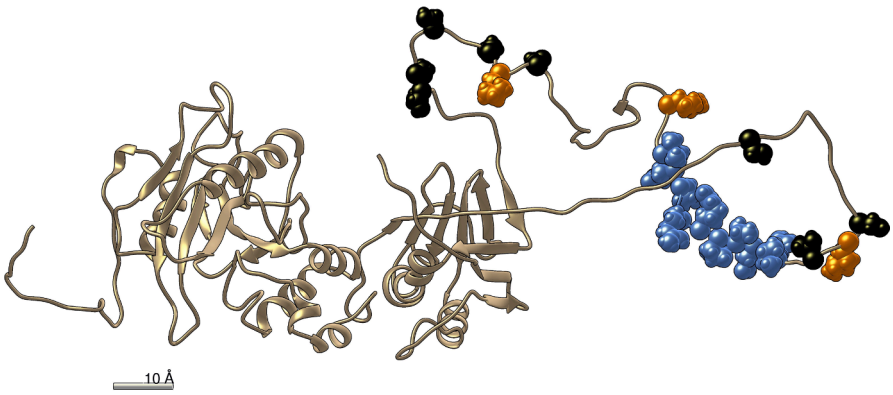

Fig. 6. Post-translational modifications in the IDR2 region. The best hSuFu model obtained from our SAXS data is represented showing phosphorylatable serines 290, 301, 342, 346, 349, 352 and threonines 305 and 353 are coloured black; ubiquitylated lysines 303, 321 and 344 are colored orange (Akimov et al., 2018) and nuclear export sequence (residues 308–318) is coloured blue (Zhang et al, 2017).

Alphafold2 model of hSuFu that has a supplementary beta strand and alpha helix as compared to our Dadimodo models. The helix spans residues 303–314, which is in the nuclear export signal region and could be a hint that the IDR2 may become more structured in the presence of a partner protein.

In conclusion, our biophysical studies show that the disordered region of Suppressor of Fused has different lengths and properties in insects and vertebrates. The difference between vertebrate and drosophila SuFu is further underlined by the observation that phosphorylated serines in dSuFu do not seem necessary for Hh pathway repression (Oh et al., 2015). In vertebrates, it spans large areas, allowing it to interact with post-translational modifying enzymes. Looking for partners specifically able to bind the IDR2 would help understand the role of this peculiar appendix.

Declaration of Competing Interest

The authors declare that they have no known competing financial interests or personal relationships that could have appeared to influence the work reported in this paper.

Acknowledgements

We are very grateful to Marie-Hélène Le Du, Dominique Durand and Patrice Vachette (Institut de Biologie Intégrative de la Cellule I2BC, CEA, CNRS, Université Paris-Saclay, France) for help with data processing software, the SOLEIL synchrotron for access to beamlines, Javier Perez at Swing beamline, and Frank Wien and Matthieu Réfrégiers at Disco beamline. We thank Valérie Campanacci (I2BC) and Alexandre Pozza (UMR7099, CNRS) for SEC-MALS analyses. Molecular graphics figures and analyses were performed with UCSF Chimera, developed by the Resource for Biocomputing, Visualization, and Informatics at the University of California, San Francisco, with support from NIH P41-GM103311.

Funding

AJ was financed by a thesis grant from Ministère de l'Enseignement Supérieur et de la Recherche and by a fourth year thesis grant from Association pour la Recherche contre le Cancer (ARC). SM was financed by a thesis grant from Ministère de l'Enseignement Supérieur et de la Recherche - IDEX Paris Sciences Lettres. This work was supported by the Centre National de la Recherche Scientifique, and by the "Initiative d'Excellence" program from the French State (Grant "DYNAMO", ANR-11-LABEX-0011-01) and Fondation ARC pour la recherche sur le cancer (grant 1112) to APl and MS.

Author contribution

SM, AJ and APa cloned and purified proteins. SM, AJ, AT and VB measured and processed CD and SAXS data. VB, AT, MB and FO performed molecular modelling and analysis. OR helped with Dadimodo modeling. APl and MS provided constructs and background about Hh pathway. VB designed the research, conducted research and wrote the manuscript with the help of all authors.

Appendix A. Supplementary data

Supplementary data to this article can be found online at https://doi.org/10.1016/j.jsb.2022.107853.

References

Akimov, V., Barrio-Hernandez, I., Hansen, S.V.F., Hallenborg, P., Pedersen, A.-K., Bekker-Jensen, D.B., Puglia, M., Christensen, S.D.K., Vanselow, J.T., Nielsen, M.M., Kratchmarova, I., Kelstrup, C.D., Olsen, J.V., Blagoev, B., 2018. UbiSite approach for comprehensive mapping of lysine and N-terminal ubiquitination sites. Nat. Struct. Mol. Biol. 25 (7), 631–640. https://doi.org/10.1038/s41594-018-0084-y.

Brookes, E., Vachette, P., Rocco, M., Pérez, J., 2016. US-SOMO HPLC-SAXS module: dealing with capillary fouling and extraction of pure component patterns from poorly resolved SEC-SAXS data. J. Appl. Crystallogr. 49 (5), 1827–1841. https://doi.org/10.1107/S1600576716011201.

Chen, Y., Yue, S., Xie, L., Pu, X.H., Jin, T., Cheng, S.Y., 2011. Dual phosphorylation of Suppressor of fused by PKA and GSK3beta regulates its stability and localization in the primary cilium. J Biol Chem 286, 13502–13511. https://doi.org/10.1074/jbc.M110.217604.

Cherry, A.L., Finta, C., Karlström, M., Jin, Q., Schwend, T., Astorga-Wells, J., Zubarev, R. A., Del Campo, M., Criswell, A.R., de Sanctis, D., Jovine, L., Toftgård, R., 2013. Structural basis of SUFU-GLI interaction in human Hedgehog signalling regulation. Acta Crystallogr. Sect. D 69 (12), 2563–2579. https://doi.org/10.1107/S0907444913028473.

Cooper, A.F., Yu, K.P., Brueckner, M., Brailey, L.L., Johnson, L., McGrath, J.M., Bale, A. E., 2005. Cardiac and CNS defects in a mouse with targeted disruption of suppressor of fused. Development 132, 4407–4417.

Emekli, U., Schneidman-Duhovny, D., Wolfson, H.J., Nussinov, R., Haliloglu, T., 2008. HingeProt: automated prediction of hinges in protein structures. Proteins 70 (4), 1219–1227.

Fändrich, M., Forge, V., Buder, K., Kittler, M., Dobson, C.M., Diekmann, S., 2003. Myoglobin forms amyloid fibrils by association of unfolded polypeptide segments. Proc. Natl. Acad. Sci. 100 (26), 15463–15468.

Fiser, A., Do, R.K.G., Šali, A., 2000. Modeling of loops in protein structures. Protein Sci. 9 (9), 1753–1773. https://doi.org/10.1110/ps.9.9.1753.

Franke, D., Petoukhov, M.V., Konarev, P.V., Panjkovich, A., Tuukkanen, A., Mertens, H. D.T., Kikhney, A.G., Hajizadeh, N.R., Franklin, J.M., Jeffries, C.M., Svergun, D.I., 2017. ATSAS 2.8: a comprehensive data analysis suite for small-angle scattering from macromolecular solutions. J. Appl. Crystallogr. 50, 1212–1225. https://doi.org/10.1107/S1600576717007786.

Gouet, P., Robert, X., Courcelle, E., 2003. ESPript/ENDscript: Extracting and rendering sequence and 3D information from atomic structures of proteins. Nucleic Acids Res 31, 3320–3323.

Grudinin, S., Garkavenko, M., Kazennov, A., 2017. Pepsi-SAXS: an adaptive method for rapid and accurate computation of small-angle X-ray scattering profiles. Acta cristallographica Section D 73 (5), 449–464. https://doi.org/10.1107/S2059798317005745.

Hooper, J.E., Scott, M.P., 1989. The Drosophila patched gene encodes a putative membrane protein required for segmental patterning. Cell 59 (4), 751–765.
Hornbeck, P.V., Chabra, I., Kornhauser, J.M., Skrzypek, E., Zhang, B., 2004. PhosphoSite: A bioinformatics resource dedicated to physiological protein phosphorylation. PROTEOMICS 4 (6), 1551–1561. https://doi.org/10.1002/pmic.200300772.
Hu, A., Song, B.-L., 2019. The interplay of Patched, Smoothened and cholesterol in Hedgehog signaling. Curr. Opin. Cell Biol. 61, 31–38. https://doi.org/10.1016/j.ceb.2019.06.008.
Huangfu, D., Liu, A., Rakeman, A.S., Murcia, N.S., Niswander, L., Anderson, K.V., 2003. Hedgehog signalling in the mouse requires intraflagellar transport proteins. Nature 426 (6962), 83–87. https://doi.org/10.1038/nature02061.
Ingham, P.W., Taylor, A.M., Nakano, Y., 1991. Role of the Drosophila patched gene in positional signalling. Nature 353 (6340), 184–187. https://doi.org/10.1038/353184a0.
Jabrani, A., Makamte, S., Moreau, E., Gharbi, Y., Plessis, A., Bruzzone, L., Sanial, M., Biou, V., 2017. Biophysical characterisation of the novel zinc binding property in Suppressor of Fused. Sci. Rep. 7, 11139. https://doi.org/10.1038/s41598-017-11203-2.
Jiang, J., Hui, C.-C., 2008. Hedgehog Signaling in Development and Cancer. Dev. Cell 15 (6), 801–812. https://doi.org/10.1016/j.devcel.2008.11.010.
Kaufmann, K.W., Lemmon, G.H., DeLuca, S.L., Sheehan, J.H., Meiler, J., 2010. Practically Useful: What the Rosetta Protein Modeling Suite Can Do for You. Biochemistry 49, 2987–2998. https://doi.org/10.1021/bi902153g.
Kelley, L.A., Mezulis, S., Yates, C.M., Wass, M.N., Sternberg, M.J.E., 2015. The Phyre2 web portal for protein modeling, prediction and analysis. Nat. Protoc. 10 (6), 845–858. https://doi.org/10.1038/nprot.2015.053.
Koudijs, M.J., den Broeder, M.J., Keijser, A., Wienholds, E., Houwing, S., van Rooijen, E. M.H.C., Geisler, R., van Eeden, F.J.M., Mullins, M., 2005. The Zebrafish Mutants dre, uki, and lep Encode Negative Regulators of the Hedgehog Signaling Pathway. PLoS Genet. 1 (2), e19. https://doi.org/10.1371/journal.pgen.0010019.
Lees, J.G., Smith, B.R., Wien, F., Miles, A.J., Wallace, B.A., 2004. CDtool—an integrated software package for circular dichroism spectroscopic data processing, analysis, and archiving. Anal. Biochem. 332 (2), 285–289. https://doi.org/10.1016/j.ab.2004.06.002.
Marigo, V., Davey, R.A., Zuo, Y.i., Cunningham, J.M., Tabin, C.J., 1996. Biochemical evidence that Patched is the Hedgehog receptor. Nature 384 (6605), 176–179.
Maurya, A.K., Ben, J., Zhao, Z., Lee, R.T.H., Niah, W., Ng, A.S.M., Iyu, A., Yu, W., Elworthy, S., van Eeden, F.J.M., Ingham, P.W., Mullins, M.C., 2013. Positive and Negative Regulation of Gli Activity by Kif7 in the Zebrafish Embryo. PLoS Genet. 9 (12), e1003955. https://doi.org/10.1371/journal.pgen.1003955.
Micsonai, A., Wien, F., Kernya, L., Lee, Y.-H., Goto, Y., Réfrégiers, M., Kardos, J., 2015. Accurate secondary structure prediction and fold recognition for circular dichroism spectroscopy. Proc. Natl. Acad. Sci. 112, E3095–E3103. https://doi.org/10.1073/pnas.1500851112.
Miroux, B., Walker, J.E., 1996. Over-production of proteins in Escherichia coli: mutant hosts that allow synthesis of some membrane proteins and globular proteins at high levels. J Mol Biol 260 (3), 289–298. https://doi.org/10.1006/jmbi.1996.0399.
Monecke, T., Güttler, T., Neumann, P., Dickmanns, A., Görlich, D., Ficner, R., 2009. Crystal Structure of the Nuclear Export Receptor CRM1 in Complex with Snurportin1 and RanGTP. Science 324 (5930), 1087–1091.
Monnier, V., Dussillol, F., Alves, G., Lamour-Isnard, C., Plessis, A., 1998. Suppressor of fused links Fused and Cubitus interruptus on the Hedgehog signalling pathway. Curr. Biol. 8, 583–586.
Notredame, C., Higgins, D.G., Heringa, J., 2000. T-Coffee: A novel method for fast and accurate multiple sequence alignment. J. Mol. Biol. 302, 205–217. https://doi.org/10.1006/jmbi.2000.4042.
Nüsslein-Volhard, C., Wieschaus, E., 1980. Mutations affecting segment number and polarity in Drosophila. Nature 287 (5785), 795–801.
Oh, S., Kato, M., Zhang, C., Guo, Y., Beachy, P.A., Fernandez-Zapico, M., 2015. A Comparison of Ci/Gli Activity as Regulated by Sufu in Drosophila and Mammalian Hedgehog Response. PLOS ONE 10 (8), e0135804. https://doi.org/10.1371/journal.pone.0135804.
Paces-Fessy, M., Boucher, D., Petit, E., Paute-Briand, S., Blanchet-Tournier, M.-F., 2004. The negative regulator of Gli, Suppressor of fused (Sufu), interacts with SAP18, Galectin3 and other nuclear proteins. Biochem J 378, 353–362. https://doi.org/10.1042/bj20030786.
Pak, E., Segal, R., 2016. Hedgehog Signal Transduction: Key Players, Oncogenic Drivers, and Cancer Therapy. Dev. Cell 38 (4), 333–344. https://doi.org/10.1016/j.devcel.2016.07.026.
Pettersen, E.F., Goddard, T.D., Huang, C.C., Couch, G.S., Greenblatt, D.M., Meng, E.C., Ferrin, T.E., 2004. UCSF Chimera–a visualization system for exploratory research and analysis. J Comput Chem 25 (13), 1605–1612.
Pospisilik, J.A., Schramek, D., Schnidar, H., Cronin, S.J.F., Nehme, N.T., Zhang, X., Knauf, C., Cani, P.D., Aumayr, K., Todoric, J., Bayer, M., Haschemi, A., Puviindran, V., Tar, K., Orthofer, M., Neely, G.G., Dietzl, G., Manoukian, A., Funovics, M., Prager, G., Wagner, O., Ferrandon, D., Aberger, F., Hui, C.-C., Esterbauer, H., Penninger, J.M., 2010. Drosophila Genome-wide Obesity Screen Reveals Hedgehog as a Determinant of Brown versus White Adipose Cell Fate. Cell 140 (1), 148–160. https://doi.org/10.1016/j.cell.2009.12.027.
Preat, T., 1992. Characterization of Suppressor of fused, a Complete Suppressor of the fused Segment Polarity Gene of Drosophila melanogaster. Genetics 132, 725–736.
Raducu, M., Fung, E., Serres, S., Infante, P., Barberis, A., Fischer, R., Bristow, C., Thézénas, M.-L., Finta, C., Christianson, J.C., Buffa, F.M., Kessler, B.M., Sibson, N.R., Di Marcotullio, L., Toftgård, R., D'Angiolella, V., 2016. SCF (Fbxl17) ubiquitylation of Sufu regulates Hedgehog signaling and medulloblastoma development. EMBO J. 35, 1400–1416. https://doi.org/10.15252/embj.201593374.
Rambo, R.P., Tainer, J.A., 2013. Accurate assessment of mass, models and resolution by small-angle scattering. Nature 496 (7446), 477–481. https://doi.org/10.1038/nature12070.
Rudenko, O., Thureau, A., Perez, J., 2019. In: Evolutionary refinement of the 3D structure of multi-domain protein complexes from small angle X-ray scattering data. Prague, Czech Republic, pp. 401–402. https://doi.org/10.1145/3319619.3322002.
Ruppert, J.M., Kinzler, K.W., Wong, A.J., Bigner, S.H., Kao, F.T., Law, M.L., Seuanez, H. N., O'Brien, S.J., Vogelstein, B., 1988. The GLI-Kruppel family of human genes. Mol. Cell. Biol. 8 (8), 3104–3113. https://doi.org/10.1128/MCB.8.8.3104.
Šali, A., Blundell, T.L., 1993. Comparative protein modelling by satisfaction of spatial restraints. J. Mol. Biol. 234 (3), 779–815. https://doi.org/10.1006/jmbi.1993.1626.
Schneidman-Duhovny, D., Hammel, M., Tainer, J., Sali, A., 2013. Accurate SAXS Profile Computation and its Assessment by Contrast Variation Experiments. Biophys. J. 105 (4), 962–974. https://doi.org/10.1016/j.bpj.2013.07.020.
Shannon, C.E., Weaver, W., 1949. The mathematical theory of communication. University of Illinois, Urbana.
Sisson, B.E., Ziegenhorn, S.L., Holmgren, R.A., 2006. Regulation of Ci and Su(fu) nuclear import in Drosophila. Dev. Biol. 294 (1), 258–270.
Svärd, J., Henricson, K.H., Persson-Lek, M., Rozell, B., Lauth, M., Bergström, Å., Ericson, J., Toftgård, R., Teglund, S., 2006. Genetic Elimination of Suppressor of Fused Reveals an Essential Repressor Function in the Mammalian Hedgehog Signaling Pathway. Dev. Cell 10 (2), 187–197.
Thureau, A., Roblin, P., Perez, J., 2021. BioSAXS on SWING beamline at Synchrotron SOLEIL. J. Appl. Crystallogr. 54 https://doi.org/10.1107/S1600576721008736.
Tunyasuvunakool, K., Adler, J., Wu, Z., Green, T., Zielinski, M., Žídek, A., Bridgland, A., Cowie, A., Meyer, C., Laydon, A., Velankar, S., Kleywegt, G.J., Bateman, A., Evans, R., Pritzel, A., Figurnov, M., Ronneberger, O., Bates, R., Kohl, S.A.A., Potapenko, A., Ballard, A.J., Romera-Paredes, B., Nikolov, S., Jain, R., Clancy, E., Reiman, D., Petersen, S., Senior, A.W., Kavukcuoglu, K., Birney, E., Kohli, P., Jumper, J., Hassabis, D., 2021. Highly accurate protein structure prediction for the human proteome. Nature 596 (7873), 590–596. https://doi.org/10.1038/s41586-021-03828-1.
Wang, Y., Li, Y., Hu, G., Huang, X., Rao, H., Xiong, X., Luo, Z., Lu, Q., Luo, S., 2016. Nek2A phosphorylates and stabilizes SuFu: A new strategy of Gli2/Hedgehog signaling regulatory mechanism. Cell. Signal. 28 (9), 1304–1313. https://doi.org/10.1016/j.cellsig.2016.06.010.
Yabut, O., Fernandez, G., Huynh, T., Yoon, K., Pleasure, S., 2015. Suppressor of Fused Is Critical for Maintenance of Neuronal Progenitor Identity during Corticogenesis. Cell Rep. 12 (12), 2021–2034. https://doi.org/10.1016/j.celrep.2015.08.031.
Zhang, D., Iyer, L.M., Aravind, L., 2011. A novel immunity system for bacterial nucleic acid degrading toxins and its recruitment in various eukaryotic and DNA viral systems. Nucl. Acids Res. 39, 4532–4552.
Zhang, Y., Bulkley, D.P., Xin, Y., Roberts, K.J., Asarnow, D.E., Sharma, A., Myers, B.R., Cho, W., Cheng, Y., Beachy, P.A., 2018. Structural Basis for Cholesterol Transport-like Activity of the Hedgehog Receptor Patched. Cell 175 (5), 1352–1364.e14. https://doi.org/10.1016/j.cell.2018.10.026.
Zhang, Y., Fu, L., Qi, X., Zhang, Z., Xia, Y., Jia, J., Jiang, J., Zhao, Y., Wu, G., 2013. Structural insight into the mutual recognition and regulation between Suppressor of Fused and Gli/Ci. Nat. Commun. 4, 1–12. https://doi.org/10.1038/ncomms3608.
Zhang, Z., Shen, L., Law, K., Zhang, Z., Liu, X., Hua, H., Li, S., Huang, H., Yue, S., Hui, C.-C., Cheng, S.Y., 2017. Suppressor of Fused chaperones Gli proteins to generate transcriptional responses to Sonic Hedgehog signaling. Mol. Cell. Biol. 37, e421 https://doi.org/10.1128/MCB.00421-16.